

Green-Emitting Oxonitridoberyllsilicate Ba[BeSiON₂]:Eu²⁺ for Wide Gamut Displays

Tobias Gifftthaler, Philipp Strobel, Volker Weiler, Arthur Haffner, Andreas Neuer, Jennifer Steinadler, Thomas Bräuniger, Simon D. Kloß, Stefan Rudel, Peter J. Schmidt, and Wolfgang Schnick*

Light-emitting diodes (LEDs) producing pure, highly saturated colors are the industry standard for efficient backlighting of high-color gamut displays. Vivid color reproduction, matching the eye's perception of nature, is the central paradigm in the design of narrow-band emitting phosphors. To cover a wide range of naturally occurring color tones, expansion of the color gamut in the green spectral region, and therefore an advanced applicable green phosphor, is highly desired. Herein, the oxonitridoberyllsilicate Ba[BeSiON₂]:Eu²⁺ showing outstanding narrow-band green emission ($\lambda_{\max} \approx 526$ nm with FWHM ≈ 1600 cm⁻¹ (≈ 45 nm), $x = 0.212$, $y = 0.715$) when excited with InGaN-based blue LEDs is presented. High quantum efficiency and low thermal quenching (>90% rel. quantum efficiency at 100 °C) as well as excellent scalability make the material suitable for industrial application in high color-gamut LED displays. A prototype phosphor-converted-LED (pc-LED), with green-emitting Ba[BeSiON₂]:Eu²⁺ and K₂SiF₆:Mn⁴⁺ as red phosphor shows an extraordinary coverage in the CIE 1931 color space of 109% compared to the DCI-P3 standard, topping the widely applied β -SiAlON:Eu²⁺ phosphor (104%), making it suitable for use in phone displays, monitors, and television screens.

LEDs as well as quantum dot converted inorganic LEDs (QLED) and phosphor converted inorganic LEDs (pcLED) are competing for the lead in overall applicability. While organic-LED-based displays feature high color gamuts and are therefore often used in miniaturized displays, they have major drawbacks such as rather high energy consumption, limited luminance, and reduced front of screen brightness.^[1-4] In contrast, inorganic semiconductor-based LEDs have a comparably low energy consumption and long lifespan, and are increasingly available as mini and micro LEDs either as direct emitters or as backlight for liquid crystal displays (LCD), which makes them suitable for miniaturized pixelated displays.^[5-11] In application are either a combination of primary red, green, and blue LEDs or, more efficiently, a blue LED combined with color down-converters. In the latter, color conversion is usually achieved with quantum dots, which suffer from reliability

challenges and achievable brightness, or with inorganic phosphors, which have high efficacies and are thus used in illumination devices.^[12,13] Commonly used phosphor converters are though broad band emitters and hence not all specific colors can be targeted individually at high efficiency, reducing color saturation.^[14-18]

This leads to limited color gamuts in display technology making them inadequate for application, where the currently most advantageous combination for backlit LC displays, as defined above, features blue emitting InGaN primary LEDs with a combination of β -SiAlON:Eu²⁺ phosphor for green emission and K₂SiF₆:Mn⁴⁺ (PSF) for red emission.^[19,20] This combination still lacks in coverage of common standardized color spaces and Pointer's gamut, the representation of natural occurring colors, as well as in efficiency. Therefore, the development of green phosphors combining high quantum efficiency (QE) with strong blue light absorption and a narrow band emission with a maximum in the region of 530 nm is imperative to increase the gamut and color saturation enabling it to compete with current state-of-the-art displaying devices. Currently, no commercialized green phosphor fulfills all criteria and candidate materials under investigation such as Eu²⁺ doped oxonitridosilicates, lithosilicates, borates,

1. Introduction

In search for next generation displaying technologies direct emitting LEDs as organic LEDs (OLED) and inorganic mini and micro

T. Gifftthaler, A. Haffner, A. Neuer, J. Steinadler, T. Bräuniger, S. D. Kloß, S. Rudel, W. Schnick
Department of Chemistry
University of Munich (LMU)
Butenandtstraße 5-13, 81377 Munich, Germany
E-mail: wolfgang.schnick@uni-muenchen.de
P. Strobel, V. Weiler, P. J. Schmidt
Lumileds Germany GmbH
Lumileds Phosphor Center Aachen
Philipsstraße 8, 52068 Aachen, Germany

 The ORCID identification number(s) for the author(s) of this article can be found under <https://doi.org/10.1002/adom.202302343>

© 2023 The Authors. Advanced Optical Materials published by Wiley-VCH GmbH. This is an open access article under the terms of the Creative Commons Attribution-NonCommercial-NoDerivs License, which permits use and distribution in any medium, provided the original work is properly cited, the use is non-commercial and no modifications or adaptations are made.

DOI: 10.1002/adom.202302343

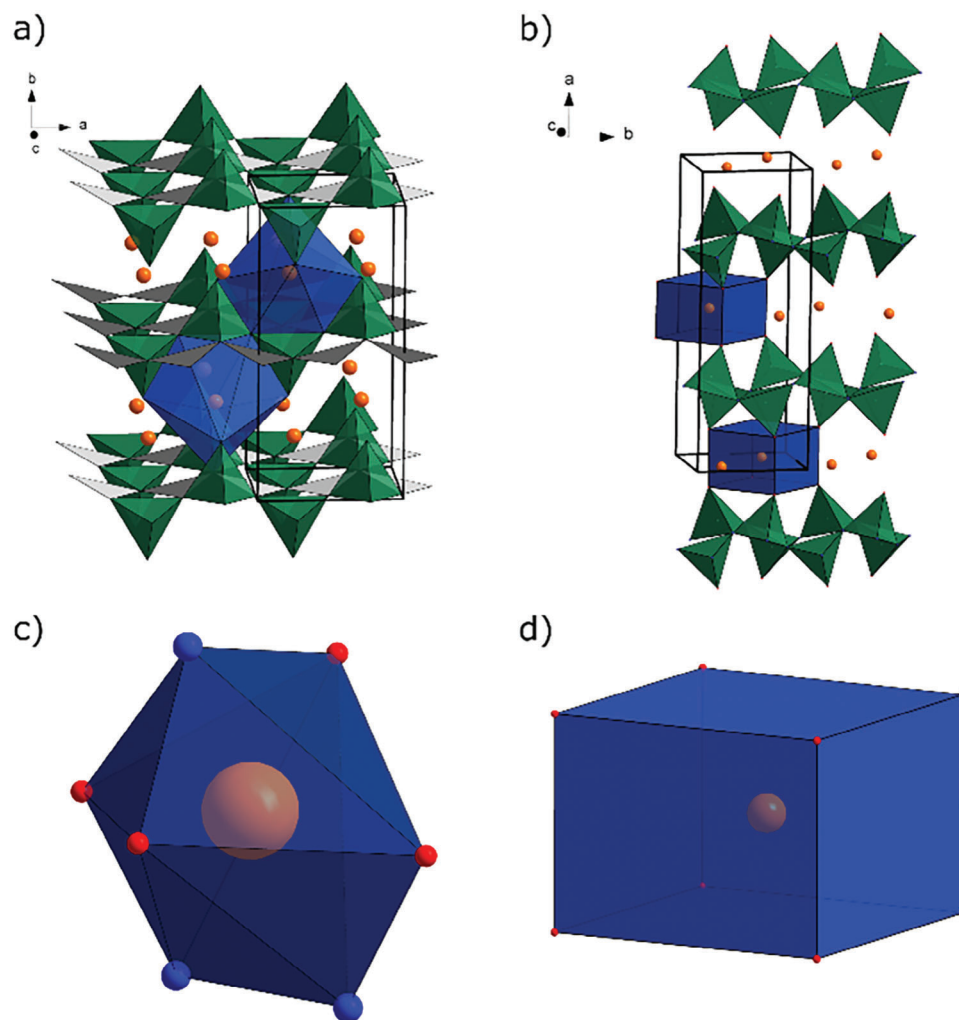


Figure 1. Comparison of schematic crystal structures of $\text{Ba}[\text{BeSiON}_2]:\text{Eu}^{2+}$ (left) to $\text{BaSi}_2\text{O}_2\text{N}_2$ (right). a) Layers of $[\text{SiON}_3]$ -tetrahedra (green) and trigonal planar $[\text{BeN}_3]$ -units (gray) stacked along $[010]$ with Ba ions (orange) and their respective coordinational environment ions (blue), b) Layers of $[\text{SiON}_3]$ -tetrahedra (green) stacked along $[100]$ with Ba ions (orange) and their respective coordinational environment ions (blue), c) Sevenfold oxygen (red) and nitrogen (blue) coordinated Ba ions (orange) and their coordinational environment (blue) d) Eightfold oxygen (red) coordinated Ba ions (orange) and their coordinational environment (blue).

alumolithionitridosilicates or manganese doped aluminates each suffer from low efficiency, insufficient stability, demanding synthetic accessibility or emission mismatch and are therefore not suitable to replace $\beta\text{-SiAlON}:\text{Eu}^{2+}$ in application.^[21–33]

In the design of a new Eu^{2+} -based phosphor, the focus lies on the activator's coordination geometry and type of ligand, as it defines the desired excitation and emission wavelengths.^[34] The most promising materials classes in this field, i.e., silicates, aluminosilicates, and lithosilicates, show a distinct structural motif in building corner sharing MO_4 tetrahedra connected via bridging O atoms. This leads to a broad diversity of possible structures, as linkages can be found in one, two, or all three dimensions resulting in chains, layers, or interconnected networks. The incorporation of nitrogen in silicates, hence, going from silicates to nitridosilicates, expands the variety of possible linkages from twofold coordinated oxygen to threefold or even higher coordinated nitrogen. Adding Be^{2+} , similar sized to Si^{4+} , increases the

structural variety even further, as their coordination in either tetrahedral $[\text{BeX}_4]$ or trigonal planar $[\text{BeX}_3]$ building blocks create new structural motifs and hereby, new coordination geometries for activator ions, in this case, Eu^{2+} .^[35–37] Generally, in coordination of Eu^{2+} , smaller distances, and ligands with stronger ligand fields typically lead to higher energetic splitting $\text{Eu}:5d$ states and therefore, to lower energetic absorption transitions. This adds to the nephelauxetic effect, lowering the energies of $\text{Eu}:5d$ states due to more covalent bonding characteristics. In this case, the substitution of O by N in a coordination sphere eventually leads to an emission shift towards the red spectral region for a given Stokes shift.

Here, we report the novel green emitting oxonitridoberylosilicate phosphor $\text{Ba}[\text{BeSiON}_2]:\text{Eu}^{2+}$ (BBS), which we characterize regarding its luminescence properties, chemical composition, and structure, showing that it is suitable for LEDs with high color gamut.

2. Results and Discussion

2.1. Synthesis and Chemical Analysis

The high-temperature synthesis of $\text{Ba}[\text{BeSiON}_2]:\text{Eu}^{2+}$ (BBS) yields an air and moisture resistant yellow-greenish powder, which dissolves slowly in diluted hydrochloric acid. The structure of BBS was solved and refined based on single-crystal X-ray diffraction data (SCXRD) and confirmed with Rietveld refinement of powder X-ray diffraction data (PXRD, Figure S1, Tables S1,S2, Supporting Information). The chemical composition was confirmed by a combination of energy dispersive X-ray spectroscopy (EDS) (averaged over eight datapoints: $\text{Ba}_{1.0}[\text{BeSi}_{0.9(1)}\text{O}_{1.1(3)}\text{N}_{2.0(5)}]$) and nuclear magnetic resonance spectroscopy (NMR) data. Since Be is hardly detectable by EDS, its presence was verified by NMR measurements. The observed characteristic line shape of the central transition broadened by the quadrupolar interaction is in good agreement with the structural motif of trigonal planar coordination for the Be site (details in Supporting Information).

2.2. Crystal Structure Determination

$\text{Ba}[\text{BeSiON}_2]$ crystallizes in the orthorhombic space group $\text{Ama}2$ (no. 40) with lattice parameters $a = 5.6366(3)$, $b = 11.6363(7)$ and $c = 4.9295(3)$ Å.^[38] It exhibits $[\text{BeSiON}_2]^{2-}$ layers built by alternating chains of condensed trigonal planar $[\text{BeN}_3]^{7-}$ units and $[\text{SiON}_3]^{7-}$ tetrahedra. These tetrahedral chains show a strictly alternating up-down-up-down sequence, as shown in Figure 1. The chemically preferred occupation of the terminal position by O was also indicated by SCXRD refinement, as given with smaller interatomic distances compared to N-occupied positions.^[39] All Ba^{2+} ions share one crystallographic site located between the $[\text{BeSiON}_2]^{2-}$ layers, sevenfold coordinated by four O and three N atoms forming a distorted pentagonal bipyramid. The interatomic distances are found between 2.64 and 2.83 Å for Ba–O and 2.95–2.99 Å for Ba–N, respectively. Further crystallographic details are given in the Tables S3,S4 (Supporting Information).

The crystal structure is closely related to that of $\text{Ba}[\text{Si}_2\text{O}_2\text{N}_2]$ crystallizing in space group Pbcn , as shown in Figure 1.^[40] but in $\text{Ba}[\text{BeSiON}_2]$ every second $[\text{SiON}_3]^{7-}$ tetrahedron is replaced by a $[\text{BeN}_3]^{7-}$ unit.

The substitution leads to a reduction of the Si–Si distance between respective layers from 7.2 to 5.8 Å, while the degree of condensation κ (atomic ratio of tetrahedral centers to coordinating atoms) rises from 1/2 to 2/3. The coordination of Ba significantly changes from a cuboid shaped eightfold coordination by O in $\text{Ba}[\text{Si}_2\text{O}_2\text{N}_2]$ to irregularly sevenfold coordination by O and N in BBS.

2.3. UV/Vis Spectroscopy

Diffuse reflectance UV–vis spectra of undoped samples were collected to determine the optical band gap of BBS. The collected reflectance spectra were converted to pseudo absorption spectra using the Kubelka–Munk-theory and displayed in a Tauc-plot (see Figure S5, Supporting Information).^[41–42] The zero point of a linear data fit on the inflection point determined the, assumed direct, band gap to be around 4.0 eV. This is within the usual range

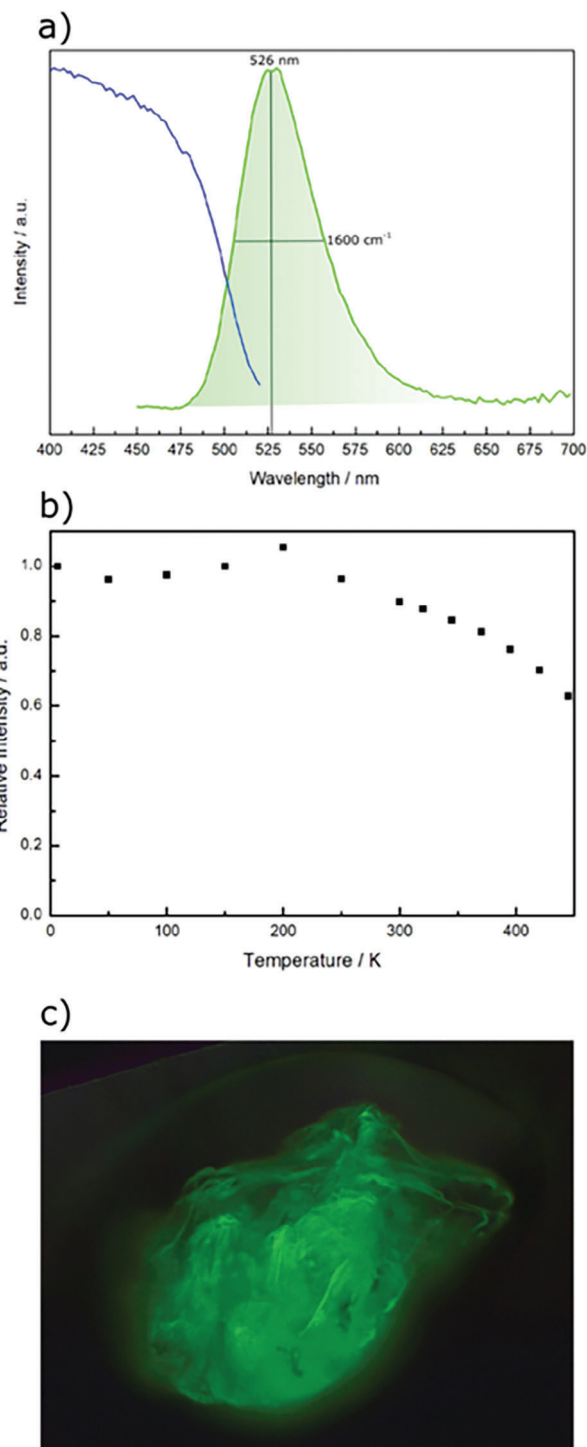


Figure 2. Luminescence of $\text{Ba}[\text{BeSiON}_2]:\text{Eu}^{2+}$. a) Excitation (blue) and emission (green) curves of selected particles of $\text{Ba}[\text{BeSiON}_2]:\text{Eu}^{2+}$, b) Thermal quenching behavior of $\text{Ba}[\text{BeSiON}_2]:\text{Eu}^{2+}$, normalized on the intensity at 6 K, c) Microscopic image of agglomerated crystals of $\text{Ba}[\text{BeSiON}_2]:\text{Eu}^{2+}$ under UV light.

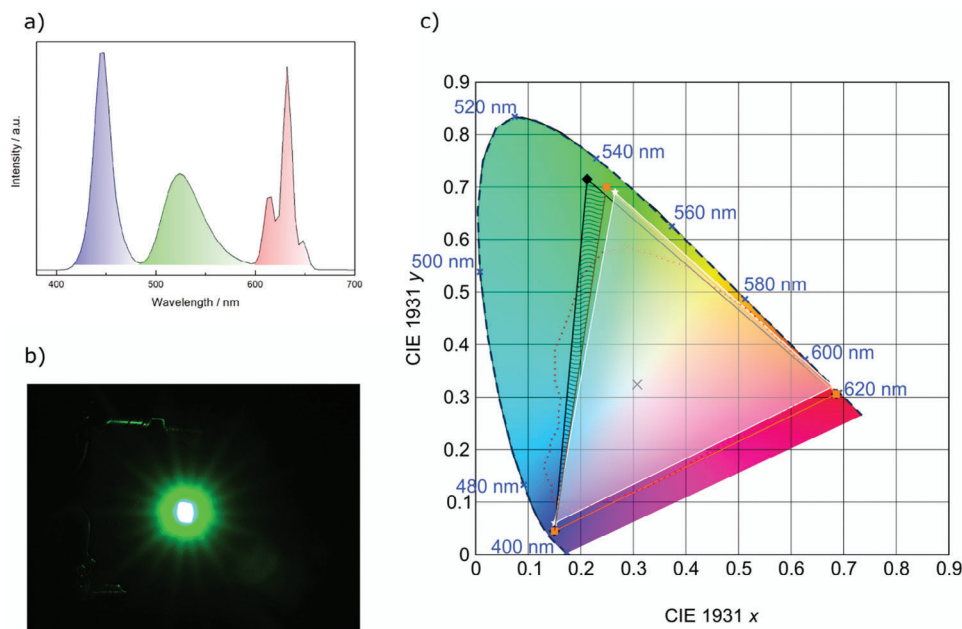


Figure 3. Emission of a LED chip with Ba[BeSiON₂]:Eu²⁺. a) Simulated emission diagram of a InGaN LED (blue) with Ba[BeSiON₂]:Eu²⁺ (green) and PSF (red). b) Image of a InGaN pcLED with Ba[BeSiON₂]:Eu²⁺ c) CIE 1931 diagram of a display with a pcLED (BBS+PSF) as background light source. The black triangle being the covered gamut area, the orange triangle the covered area with β -SiAlON as green phosphor. The gained gamut coverage is given as the striped area. For reference Pointer's gamut (red dotted area) and DCI-P3 standard (white triangle) are given.

for (oxo-)nitridic phosphors, but smaller than the band gap of Ba[Si₂O₂N₂] at 4.8 eV.^[40,43]

2.4. Luminescence

The different coordination environments of Ba between Ba[Si₂O₂N₂] and BBS, as shown in Figure S2 (Supporting Information), lead to different luminescence properties, as Eu²⁺ is assumed to replace Ba²⁺ statistically. BBS shows an emission maximum at a longer wavelength (526 nm) compared to 490 nm of Ba[Si₂O₂N₂]:Eu²⁺, and therefore emits green light.^[44]

BBS shows green luminescence under irradiation of UV to blue light, due to the Eu²⁺ 4f⁷(⁸S_{7/2}) → 4f⁶(⁷F)5d¹ transition (see Figure 2c). Accordingly, the emission shows a maximum at 526 nm with a full width at half maximum (FWHM) of 45 nm (≈1600 cm⁻¹), as given in Figure 2a for BBS with 0.75% nominal dopant concentration. The additionally shown excitation curve drops significantly only in the spectral region beyond 475 nm. Thus, efficient excitation can be obtained with blue emitting primary LEDs. And the ideal excitation can be realized with an UV- or a blue LED chip (≈450 nm), as required for display backlighting applications. A variation of the dopant concentration leads to an emission shift (see Figure S6, Supporting Information), likely due to the influence of the different ionic radii of Eu²⁺ and Ba²⁺ on the host lattice.^[45]

As given in Figure 2b the temperature-dependent photoluminescence emission intensity of BBS, defined as the ratio of emitted to absorbed photons normalized to the value at 6 K, decreases with temperature. With a maximum at 200 K, the relative QE is still above 90% at 300 K compared to the low temperature QE and contains more than 70% up to 400 K. The emission wavelength

does not change during heating. Temperature dependent spectra are given in the supporting information (Figures S7,S8, Supporting Information). The internal quantum efficiency (IQE), representing the ratio of emitted to absorbed photons, was found to be up to 43% for as-synthesized samples. This can be further increased for industrial application by optimization of the synthetic process, as variation of the thermal parameters and mechanical treatment are highly influential on crystallite growth and therefore absorption and emission.

A green LED suitable for display backlighting application was built (depicted in Figure 3b) and relevant luminescence properties were measured. Hereby, the standard design for backlight LEDs was used. A blue emitting InGaN LED acts as primary emitter covered with a green emitting phosphor, in this case BaBeSiON₂:Eu²⁺. For demonstration of applicability a simulation of the emitted light and applied filters is used to obtain the individual RGB spectra (see Figure S9, Supporting Information). Every given color displayable by this setup can be described as a combination of the three individually emitted color points via a coordinate in a CIE color diagram. The main goal in application is to widen the so-called color gamut, hence, the coverage of predefined color spaces, focusing on the green spectral region, where a wider gamut is most beneficial. The color spaces used for benchmarking are the established NTSC color space developed for TV applications as well as the newer DCI-P3 and Rec.2020 focusing on modern displays.^[46,47]

When BBS (x = 0.212, y = 0.715) is used in combination with a blue emitting LED chip with PSF as red phosphor, the color gamut covers the visible spectrum (see Figure 3a) as well as 109.0% of the DCI-P3 standard (108.3% compared to NTSC, 80.2% to Rec.2020), as shown in Figure 3c. This marks a major increase compared to the 104.4% (103.7% NTSC) of the widely

used standard green emitting phosphor β -SiAlON:Eu²⁺ in an equivalent configuration. This increase is due to coverage of a significantly wider variety of colors in the turquoise-green spectral region.

3. Conclusion

In conclusion, combination of narrow green emission (526 nm peak emission, FWHM = 1600 cm⁻¹) with chemical and thermal stability, as provided by Ba[BeSiON₂]:Eu²⁺, is unmatched in phosphors for application in inorganic LED backlit LC displays with high color gamut. The straightforward synthesis from commercially available starting materials meets industrial requirements and gives room for even further improvements regarding the crystallite growth and therefore, the already outstanding emission properties. For further understanding of these emission properties, theoretical and detailed experimental examinations of the electronic structure will be reported in the near future.

As energy consumption and longevity of electronics are a major concern, displays using mini-LED backlighting systems are advantageous compared to other backlighting technologies. However, already commercially available displays leave room for improvement regarding chromaticity and energy efficiency. Our material can help to improve the next generation of these displays, by reducing the percentage of color-filter erased wavelengths and therefore the overall energy loss. Furthermore, it expands the possible display color gamut especially in the very relevant green spectral region. This is crucial, as the human eye's sensitivity for green color shades is high and a variety of natural colors relies on an expanded green gamut for natural representation and leads to possible applications in displays, as in automotive or handheld devices, where wide gamut and natural color representation are highly desired. This is of particular significance, i.e., for photography and cinematography, which require high quality wide gamut displays.

In general, the incorporation of Be²⁺ as network building ion gives room for expanded research in phosphor materials, applying diversified structural motifs as a combination of trigonal planar and tetrahedral units and will prove beneficial in future phosphor design.

Further details of the crystal structure investigation(s) may be obtained from the Fachinformationszentrum Karlsruhe, 76344 Eggenstein-Leopoldshafen (Germany), on quoting the depository number CSD-2191356.

Supporting Information

Supporting Information is available from the Wiley Online Library or from the author.

Acknowledgements

The authors thank Constantin Hoch for recording the single-crystal X-ray data, Lisa Gamperl for SEM imaging, Mirjam Zipkat for assistance and Christian Minke for performing the solid-state NMR as well as the EDS measurements (all at Department of Chemistry at LMU Munich). The authors thank Hans-Helmut Bechtel (Lumileds) for spectral analysis.

Open access funding enabled and organized by Projekt DEAL.

Conflict of Interest

The authors declare no conflict of interest.

Data Availability Statement

The data that support the findings of this study are available in the supplementary material of this article.

Keywords

beryllium, ceramics, luminescence, nitrides, silicates

Received: October 9, 2023

Revised: November 8, 2023

Published online:

- [1] R. Gómez-Bombarelli, J. Aguilera-Iparraguirre, T. D. Hirzel, D. Duvenaud, D. Maclaurin, M. A. Blood-Forsythe, H. S. Chae, M. Einzinger, D.-G. Ha, T. Wu, G. Markopoulos, S. Jeon, H. Kang, H. Miyazaki, M. Numata, S. Kim, W. Huang, S. I. Hong, M. Baldo, R. P. Adams, A. Aspuru-Guzik, *Nat. Mater.* **2016**, *15*, 1120.
- [2] X. Tang, L.-S. Cui, H.-C. Li, A. J. Gillett, F. Auras, Y.-K. Qu, C. Zhong, S. T. E. Jones, Z.-Q. Jiang, R. H. Friend, L.-S. Liao, *Nat. Mater.* **2020**, *19*, 1332.
- [3] C. W. Tang, S. A. Vanslyke, *Appl. Phys. Lett.* **1987**, *51*, 913.
- [4] C. Féry, B. Racine, D. Vaufrey, H. Doyeux, S. Cinà, *Appl. Phys. Lett.* **2005**, *87*, 213502.
- [5] V. W. Lee, N. Twu, I. Kymissis, *Inf. Disp.* **2016**, *32*, 16.
- [6] T. Zhan, K. Yin, J. Xiong, Z. He, S.-T. Wu, *iScience* **2020**, *23*, 101397.
- [7] E. Quesnel, A. Lagrange, M. Vigier, M. Consonni, M. Tournaire, V. Le Marchand, A. Suhm, P. Demars, J.-C. Pillet, B. Ben Bakir, N. Olivier, E. Feltin, J. M. Lamy, M. D'amico, E. Cao, G. Haas, L. Charrier, P. Coni, *J. Soc. Inf. Disp.* **2020**, *29*, 3.
- [8] Y. Huang, G. Tan, F. Gou, M.-C. Li, S.-L. Lee, S.-T. Wu, *J. Soc. Inf. Disp.* **2019**, *27*, 387.
- [9] K. Behrman, I. Kymissis, *Nat. Electron.* **2022**, *5*, 564.
- [10] J. Shin, H. Kim, S. Sundaram, J. Jeong, B.-I. Park, C. S. Chang, J. Choi, T. Kim, M. Saravanapavanantham, K. Lu, S. Kim, J. M. Suh, K. S. Kim, M.-K. Song, Y. Liu, K. Qiao, J. H. Kim, Y. Kim, J.-H. Kang, J. Kim, D. Lee, J. Lee, J. S. Kim, H. E. Lee, H. Yeon, H. S. Kum, S.-H. Bae, V. Bulovic, K. J. Yu, K. Lee, et al., *Nature* **2023**, *614*, 81.
- [11] Y. Wu, J. Ma, P. Su, L. Zhang, B. Xia, *Nanomaterials* **2020**, *10*, 2482.
- [12] E. Jang, S. Jun, H. Jang, J. Lim, B. Kim, Y. Kim, *Adv. Mater.* **2010**, *22*, 3076.
- [13] P. Pust, P. J. Schmidt, W. Schnick, *Nat. Mater.* **2015**, *14*, 454.
- [14] P. Pust, V. Weiler, C. Hecht, A. Tücks, A. S. Wochnik, A.-K. Henß, D. Wiechert, C. Scheu, P. J. Schmidt, W. Schnick, *Nat. Mater.* **2014**, *13*, 891.
- [15] Z. Xia, A. Meijerink, *Chem. Soc. Rev.* **2017**, *46*, 275.
- [16] K. Uheda, N. Hirosaki, Y. Yamamoto, A. Naito, T. Nakajima, H. Yamamoto, *Electrochem. Solid-State Lett.* **2006**, *9*, H22.
- [17] H. Watanabe, N. Kijima, *J. Alloys Compd.* **2009**, *475*, 434.
- [18] M. Zeuner, P. J. Schmidt, W. Schnick, *Chem. Mater.* **2009**, *21*, 2467.
- [19] X. Zhang, M.-H. Fang, Y.-T. Tsai, A. Lazarowska, S. Mahlik, T. Lesniewski, M. Grinberg, W. K. Pang, F. Pan, C. Liang, W. Zhou, J. Wang, J.-F. Lee, B.-M. Cheng, T.-L. Hung, Y.-Y. Chen, R.-S. Liu, *Chem. Mater.* **2017**, *29*, 6781.
- [20] H. S. Kim, K.-I. Machida, M. Itoh, H. Hanzawa, *ECSJ. Solid State Sci. Technol.* **2014**, *3*, R234.

- [21] M.-H. Fang, C. O. M. Mariano, K.-C. Chen, J.-C. Lin, Z. Bao, S. Mahlik, T. Lesniewski, K.-M. Lu, Y.-R. Lu, Y.-J. Wu, H.-S. Sheu, J.-F. Lee, S.-F. Hu, R.-S. Liu, J. P. Attfield, *Chem. Mater.* **2021**, *33*, 1893.
- [22] M.-H. Fang, C. O. M. Mariano, P.-Y. Chen, S.-F. Hu, R.-S. Liu, *Chem. Mater.* **2020**, *32*, 1748.
- [23] H. Liao, M. Zhao, Y. Zhou, M. S. Molokeev, Q. Liu, Q. Zhang, Z. Xia, *Adv. Funct. Mater.* **2019**, *29*, 1901988.
- [24] E. H. Song, Y. Y. Zhou, Y. Wei, X. X. Han, Z. R. Tao, R. L. Qiu, Z. G. Xia, Q. Y. Zhang, *J. Mater. Chem. C* **2019**, *7*, 8192.
- [25] X. Wang, E. Song, L. Qin, D. Gui, Z. Xu, J. Xie, M. Lei, H. Zhang, Y. Wang, Y. Wang, Z. Xia, W. Liu, W. Du, S. Wang, *Chem. Mater.* **2021**, *33*, 6329.
- [26] T. Takeda, N. Hirotsuki, S. Funahashi, R.-J. Xie, *Chem. Mater.* **2015**, *27*, 5892.
- [27] D. S. Wimmer, M. Seibald, D. Baumann, S. Peschke, K. Wurst, G. Heymann, D. Dutzler, A. Garcia-Fuente, W. Urland, H. Huppertz, *Eur. J. Inorg. Chem.* **2021**, *2021*, 4470.
- [28] Y. Zhu, Y. Liang, S. Liu, H. Li, J. Chen, *Adv. Opt. Mater.* **2019**, *7*, 1801419.
- [29] Y. Zhuo, S. Hariyani, J. Zhong, J. Brgoch, *Chem. Mater.* **2021**, *33*, 3304.
- [30] K. Yoshimura, H. Fukunaga, M. Izumi, K. Takahashi, R.-J. Xie, N. Hirotsuki, *Jpn. J. Appl. Phys.* **2017**, *56*, 0417011.
- [31] P. Strobel, S. Schmiechen, M. Siegert, A. Tücks, P. J. Schmidt, W. Schnick, *Chem. Mater.* **2015**, *27*, 6109.
- [32] M. Zhang, J. Wang, Q. Zhang, W. Ding, Q. Su, *Mater. Res. Bull.* **2007**, *42*, 33.
- [33] X. Zhang, H.-C. Wang, A.-C. Tang, S.-Y. Lin, H.-C. Tong, C.-Y. Chen, Y.-C. Lee, T.-L. Tsai, R.-S. Liu, *Chem. Mater.* **2016**, *28*, 8493.
- [34] R. Shafei, D. Maganas, P. J. Strobel, P. J. Schmidt, W. Schnick, F. Neese, *J. Am. Chem. Soc.* **2022**, *144*, 8038.
- [35] R. D. Shannon, *Acta Crystallogr., Sect. A* **1976**, *32*, 751.
- [36] P. Strobel, V. Weiler, P. J. Schmidt, W. Schnick, *Chem. - Eur. J.* **2018**, *24*, 7243.
- [37] L. A. Harris, H. L. Yakel, *Acta Crystallogr., Sect. B: Struct. Crystallogr. Cryst. Chem.* **1969**, *25*, 1647.
- [38] P. E. D. Morgan, *J. Mater. Sci.* **1986**, *21*, 4305.
- [39] V. Bachmann, C. Ronda, O. Oeckler, W. Schnick, A. Meijerink, *Chem. Mater.* **2009**, *21*, 316.
- [40] J. Tauc, *Mater. Res. Bull.* **1968**, *3*, 37.
- [41] P. Kubelka, F. Munk, *Z. Tech. Phys.* **1931**, *12*, 593.
- [42] X. Wang, Z. Zhao, Q. Wu, Y. Li, C. Wang, A. Mao, Y. Wang, *Dalton Trans.* **2015**, *44*, 11057.
- [43] Y. Q. Li, A. C. A. Delsing, G. De With, H. T. Hintzen, *Chem. Mater.* **2005**, *17*, 3242.
- [44] Y. X. Pan, W. Wang, G. K. Liu, S. Skanthakumar, R. A. Rosenberg, X. Z. Guo, K. K. Li, *J. Alloys Compd.* **2009**, *488*, 638.
- [45] Digital Cinema Initiatives, LLC, Digital Cinema System Specification V1.0, Digital Cinema Initiatives, LLC Member Representatives Committee, **2005**.
- [46] International Telecommunication Union, Recommendation ITU-R BT.2020, **2012**.
- [47] O. Kumberger, H. Schmidbaur, *Chem. Unserer Zeit* **1993**, *27*, 310.